Int J Adv Manuf Technol (2011) 57:945–955
DOI 10.1007/s00170-011-3347-x

ORIGINAL ARTICLE

Development of a novel ultrasonic unit for grinding of ceramic matrix composites

Bahman Azarhoushang · Taghi Tawakoli

Received: 19 January 2011 / Accepted: 20 February 2011 / Published online: 28 July 2011

Abstract Ceramic matrix composites (CMCs) are promising materials for many high-technology engineering applications in harsh and severe environments due to their superior properties. However, in spite of all advantages, the employment of CMCs has been impeded by their high machining and finishing costs. Many of recently developed CMCs are very difficult to machine with the conventional machining technology, and improvement of the existing machining process is required and crucial. To overcome the existing technological constraints in the grinding of CMCs, a special designed block sonotrode was invented (and was registered for patent). The realization of ultrasonic-assisted machining on conventional machine tools can be carried out with much less effort by means of the new invented system. The invented block sonotrode is a specially designed perforated plate and demonstrates a multi-resonant frequency behavior. Experimental results illustrate the high performance of the presented method. A significant reduction in grinding forces and surface roughness and an increase in *G*-ratio have been achieved.

Keywords Ultrasonic-assisted grinding · Block sonotrode · Ceramic matrix composite · Grinding forces · Surface roughness · Grinding temperature · Tool wear

1 Introduction

Despite its known advantages, the ultrasonic-assisted machining process has not been widely introduced into industrial environment. The main reasons for it are the difficulties in efficient superimposing of the vibrations to the workpiece or the tool. Until the present time, the ultrasonic-assisted machining was only possible for small and light parts, when vibrating the workpiece, or for small and special designed tools, when vibrating the tool. It is demonstrated that due to the changes in mechanical properties of the material, e.g., reduction in yield points, strength, and resistance to plastic deformation, efficiency of the ultrasonic-assisted machining is much higher when the vibration is superimposed on the workpiece [1–5]. In the case of ceramics, it has been reported that the critical ductile grinding depth can be increased due to the micro-change of Young's modulus *E*, material hardness *H*, and martensite phase transition rate of Al_2O_3/ZrO_2 during the grinding process can be decreased, when superimposing ultrasonic vibration on the workpiece [6, 7]. Hence, there is an abundant need for development of a proper innovative ultrasonic vibration system which is able to vibrate industrial workpieces of different sizes and weights. To address this requirement, a special designed block sonotrode was invented (and was registered for patent [8]). The realization of ultrasonic-assisted machining on conventional machine tools can be carried out with much less effort by means of the new invented system. The invented block sonotrode is a specially designed perforated plate and demonstrates a multi-resonant frequency behavior. Utilizing the invented block sonotrode, heavy and large parts can be vibrated.

Ceramic matrix composites (CMCs) are relatively new and promising materials for many high-technology engineering applications in harsh and severe environments due to their superior properties, including high strength at elevated temperatures, low thermal conductivity, corrosion resistance, excellent wear resistance, good frictional behavior, high fracture toughness, high strength to weight ratio, and low density. These properties provide considerable

B. Azarhoushang (✉) · T. Tawakoli
Institute of Grinding and Precision Technology,
KSF, Furtwangen University,
Furtwangen, Germany
e-mail: B.Azarhoushang@hs-furtwangen.de

lifetime increases over conventional metal and/or ceramics components [9].

As the sintered CMCs are very hard, the material removal processes are generally limited to machining processes with geometrically undefined cutting edges. Grinding with a diamond wheel is the most commonly used process to achieve dimensional accuracy and required surface finish of ceramic and CMCs parts. The cost for such a machining process can be as much as 60–80% of the overall manufacturing cost [10, 11]. Hence, in spite of all aforementioned advantages, the employment of CMCs has been impeded by their high machining and finishing costs. A range of new ceramic matrix composites with excellent material properties is also being developed every day for various engineering applications. Many of these new materials are very difficult to machine with the existent conventional machining technology and improvement of the existing machining process is required and crucial.

There are only few reports about the grinding of these new composites. CMC grinding is generally characterized with excessive grinding forces and temperature [12–14]. Tashiro et al. ground a C/C-SiC composite in a dry condition with various tool materials (cemented carbide K10, WA120, and D180V). It was concluded that the porous vitrified bonded diamond wheel was the most proper tool in the experiment. However, even when the diamond wheel was utilized, there were few grooves and uncut SiC areas on the workpiece, demonstrating that the material is very difficult to machine [13]. Li et al. and Weinert and Jansen, while utilizing the face grinding process for machining CMCs, have also concluded that due to the hardness of ceramic matrix, which is almost comparable with conventional abrasives, diamond abrasives are the optimum choice for machining CMC composites [12, 14]. Li et al. have introduced rotary ultrasonic machining (RUM) into face grinding of CMC materials for the first time. They found that compared with conventional diamond face grinding process, the cutting force can be reduced significantly (about 50%) and material removal rate can be improved (about 10%) with RUM.

In this investigation, an ultrasonic unit has been designed and developed to grind ceramic matrix composites ultrasonically. Grinding forces, surface roughness, surface profile, and tool wear are compared for grinding of CMC with and without superimposing of ultrasonic vibrations to the process for two types of C/SiCs. The main effects of cutting conditions on CMC grinding are also systematically studied.

1.1 Superimposing ultrasonic vibrations on the workpiece

In the following sections, the design and analysis of the invented ultrasonic unit is introduced. The block sonotrode is the most important component of the ultrasonic unit which makes the acoustic head able to vibrate heavy and large parts. In order to reach high amplitude at the surface of the block sonotrode, a high gain booster (ratio 1:2) was utilized.

1.2 Design of the acoustic head

The acoustic head (Fig. 1) is composed of a piezoelectric transducer, a booster, and the invented block sonotrode and is installed on four legs. It exhibits a longitudinal vibration mode at its operating resonance frequency. The acoustic head parts should have high fatigue resistance and low acoustic losses (meaning that they should not absorb too much energy from the vibrations). The transducer must be capable of producing sufficient force to drive the combined mass of the acoustic head and the workpiece at this condition. For a minimum vibration loss and optimal acoustic behavior, the components of the acoustic head should have the same resonance frequency. In order to reach the desired resonance frequency and to achieve longitudinal vibrations, the length of the transducer and the booster should be equal to half of the oscillations wavelength or an integer value of that. In the case of the block sonotrode, it is necessary that diameters of the holes and the holes pattern guarantee a high amplification factor and a multi-resonance behavior. In addition, the block sonotrode which also serves as a machine table must have a certain rigidity to ensure an accurate machining process. Figure 2 illustrates schematically the acoustic head along with the stress and amplitude distribution.

Finite element method (FEM) is one of the most reliable tools for analyzing the ultrasonic system. It has been established that the resonance and anti-resonance results from the Ansys software FEM model and the physical experiments are in exceptional agreement; the error is normally less than 1% [15–17]. The vibration of the combined mass can be modeled by modal analysis, to observe the vibration behavior (mode shapes and the

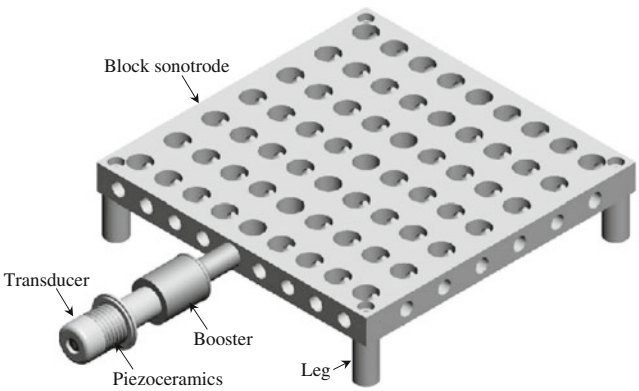

Fig. 1 The 3D model of the acoustic head

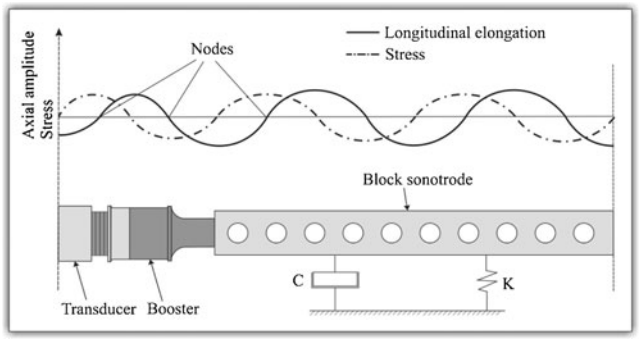

Fig. 2 Scheme of the acoustic head along with the stress and amplitude distribution

location of nodal planes), and harmonic analysis, to determine its natural frequency.

1.3 FEM analysis

Effective vibration of the acoustic head is achieved when it is used as a wave guide, at the resonance frequency, for amplification of vibration amplitude. Therefore, FEM analysis was utilized to find the optimum dimensions of components of the acoustic head, i.e., the transducer, the booster, and the block sonotrode, so that the acoustic head may reach a resonance frequency of about 20 kHz (the desired vibration condition). Each part of the acoustic head, except the back mass of the transducer which is made of steel, is made of aluminum 7075-T6 to provide enough stiffness and low acoustic losses. The favored vibration conditions were chosen to be around 20 kHz. However, due to the multi-resonant frequency behavior of the block sonotrode, for the first time it is possible to carry out experiments, on the same ultrasonic unit, with various frequencies.

The analyzed 3-KW ultrasonic transducer was composed of six PZT-4 piezoceramic rings, a cylinder-shaped back mass made of steel, and a stepped front mass made of Al 7075-T6. The bolts material was taken from steel. The booster and sonotrode are also made from aluminum alloy, Al 7075-T6. The material properties of aluminum alloy (Al 7075-T6) and steel, which are required by the Ansys software, are presented in Table 1.

The material properties of piezoceramics published by most manufacturers cannot be directly used in the Ansys software. Hence, the data should be transformed to the piezoelectric material matrices required by Ansys, e.g., dielectric relative permittivity matrix $\left[\varepsilon_{\mathrm{r}}^{\mathrm{s}}\right]$, piezoelectric stress matrix $[e]$, and compliance matrix under constant electric field [SE] or a stiffness matrix $[c]$. The following material properties have been used for the PZT-4:

Piezoelectric stress matrix:

$$[e] = \begin{bmatrix} 0 & -5.2 & 0 \\ 0 & 15.1 & 0 \\ 0 & -5.2 & 0 \\ 12.7 & 0 & 0 \\ 0 & 0 & 12.7 \\ 0 & 0 & 0 \end{bmatrix} \left(\mathrm{C/m^2}\right)$$

Stiffness matrix:

$$[c] = \begin{bmatrix} 13.9 & 7.43 & 7.78 & 0 & 0 & 0 \\ 7.43 & 11.5 & 7.43 & 0 & 0 & 0 \\ 7.78 & 7.43 & 13.9 & 0 & 0 & 0 \\ 0 & 0 & 0 & 2.56 & 0 & 0 \\ 0 & 0 & 0 & 0 & 2.56 & 0 \\ 0 & 0 & 0 & 0 & 0 & 3.06 \end{bmatrix} \times 10^{-10}\left(\mathrm{N/m^2}\right)$$

Dielectric relative permittivity matrix at constant strain:

$$\left[E_{\mathrm{r}}^{\mathrm{S}}\right] = \begin{bmatrix} 729 & 0 & 0 \\ 0 & 635 & 0 \\ 0 & 0 & 729 \end{bmatrix} (\mathrm{F/m})$$

The density of PZT-4 is 7,700 kg/m^3. The finite element approach presented in this paper was implemented by the ANSYS software. In order to evaluate the acoustic head, the optimized transducer, booster, and block sonotrode were assembled together, and the acoustic head was 3D modeled by modal and harmonic analysis. SOLID227 element was applied to piezoceramics, and SOLID98 element was utilized for other components. SOLID227 is a 3D coupled field element with a tetrahedral geometry. The element is defined by ten nodes with up to five degrees of freedom per node. It exhibits piezoelectric, piezoresistive, thermal–piezoelectric, structural–thermal, thermal–electric, and structural–thermoelectric field capabilities. Element size was set to be equal to 4 mm.

The acoustic head exhibits a multi-resonant frequency behavior due to the invented block sonotrode. One of the obtained resonance frequencies is 20 kHz. Figure 3 shows the mode shapes, location of nodes and displacement in Z-direction along the acoustic head related to the resonance frequencies at 20 kHz.

Table 1 Material properties of Al 7075-T6 and St 304

Material	AL 7075-T6	St 304
Modulus of elasticity (N/m^2)	77×10^9	207×10^9
Poisson's ratio	0.33	0.292
Density (kg/m^3)	2,810	7,868

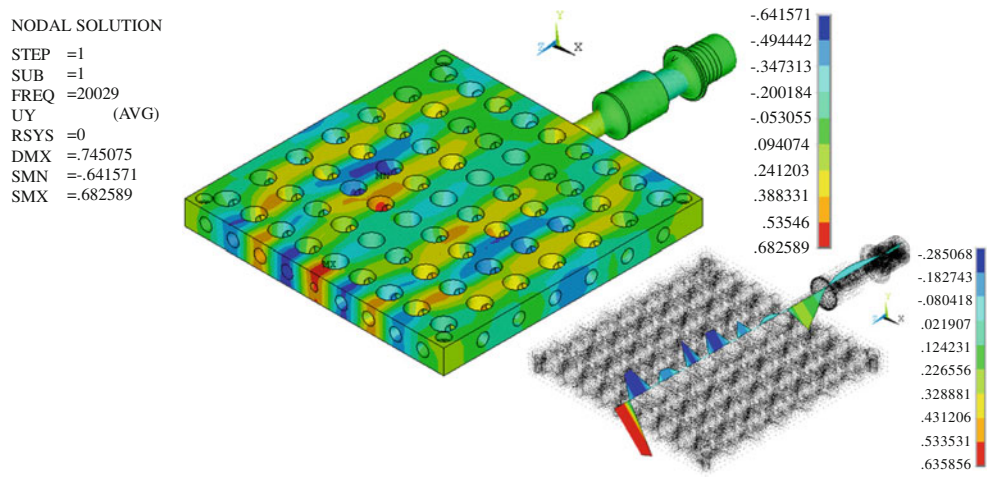

Fig. 3 Displacement of the acoustic head in *Z*-direction and location of nodes from modal analysis in 3D modeling

1.4 3D harmonic analysis

The harmonic analysis was performed to validate the modal analysis results. This is confirmed when the frequency obtained from harmonic analysis is near to or the same as the modal analysis frequency. The acoustic head was 3D modeled under no load and structural constraint. For harmonic analysis of the acoustic head, the negative poles of the piezoceramic disks were connected to zero voltage of common ground, and the positive poles were connected to 1,000 AC voltage. The positive faces of the piezoelectric rings are electrically connected together, and also the negative faces are electrically coupled together. The full method and sparse matrix (SPARSE) solver were selected for harmonic analysis as it was recommended by ANSYS Coupled-Field Analysis Guide.

The harmonic analysis was executed over a frequency breadth (0.95 to 1.05 times the frequency obtained by modal analysis) inside which the resonance frequency was expected. In order to obtain the frequency at which the highest amplitude is reached, the frequency breadth was divided into 100 steps. The steady-state response of the system to a sinusoidal varying input voltage of ±1,000 V across the piezoceramic rings is computed by the FEM software at each frequency. Frequencies obtained from harmonic analysis are demonstrated by Fig. 4. Results show a very good agreement between the modal and the harmonic analysis frequencies.

1.5 Evaluation of the FEM results

A new AMMM technology is utilized in this investigation. Many vibrating modes can be synchronously excited by the AMMM generator to produce uniform and repeatable multimode vibrations with a high intensity, while avoiding the creation of stationary and standing waves, so that the whole vibrating system is fully agitated. The AMMM generator is also able to produce variable frequency sweeping oscillations around a central operating frequency and contains an amplitude-modulated output signal (where the frequency of amplitude modulation follows sub-harmonic low frequency vibrating modes of the mechanical system) [18, 19].The AMMM generator is capable of measuring the resonance frequency within 10 and 100 kHz with a resolution of 10 Hz. The generator converts phase shifts (from −90° to 90°) to voltage in a range between 0 and 5 V. There are two different ways to show resonance behavior clearly: the amplitude resonance and the phase resonance. The former is frequently more dramatic, but the phase resonance, which is the angular shift between the external driver and the oscillating object, may sometimes be clearer. The phase of displacement oscillation relative to the driving force shifts by 180° as the driving frequency varies through resonance.

Figure 5 shows phase versus frequency diagram of the fabricated acoustic head measured by the AMMM generator. The actual value of resonance frequency and amplitude of the fabricated acoustic head, measured by the

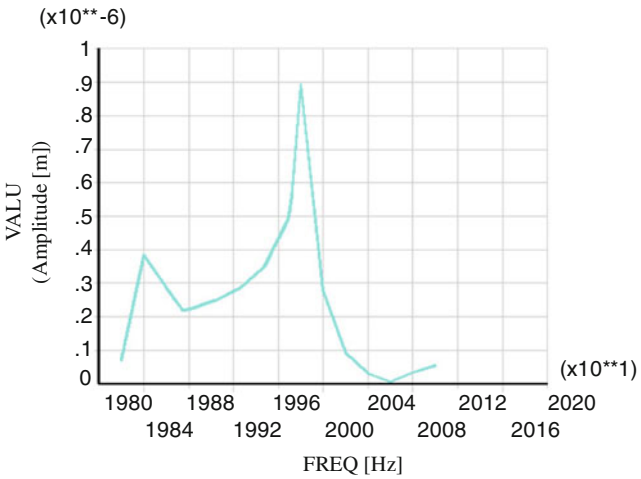

Fig. 4 Amplitude versus frequency from harmonic analysis in 3D modeling

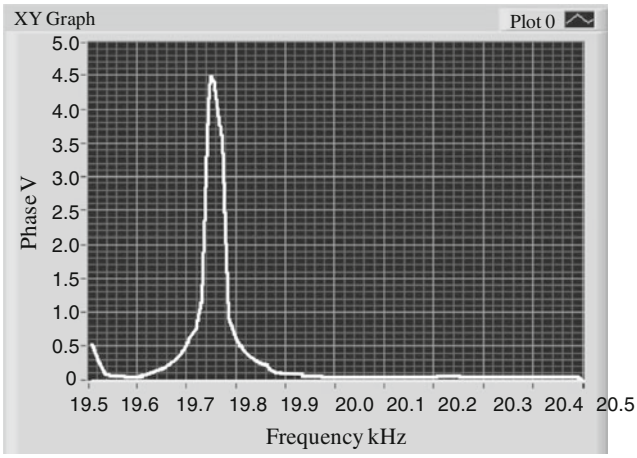

Fig. 5 The measured resonance frequency of the fabricated acoustic head

AMMM generator, are in very good agreement with the results given by the harmonic analysis. A comparison between predicted frequencies of the FEM modal analysis and the measured frequency is shown in Table 2.

Compared with the modal analysis, the predicted result by the harmonic analysis is more accurate and closer to the measured frequency. As can be seen in Fig. 4, the predicted resonance frequency by the harmonic analysis is almost 19.98 kHz. Hence, the percentage error of the harmonic analysis is 1.16%.

The vibration amplitude of the block sonotrode can be increased up to 15 μm by changing the setting on the power supply. For the first time, the fabricated acoustic head makes it possible to vibrate heavy and large parts (without modifying the parts) by employing relatively low power generator and transducer. Additionally, due to the multi-resonant frequency behavior of the block sonotrode, experiments can be carried out at various vibration frequencies.

2 Experimental setup and procedures

Figure 6 illustrates the experimental setup. The grinding forces were measured by a dynamometer which was mounted beneath the workpiece and above the machine table. The grinding wheel wear was measured by a sensing measurement system, which was integrated in the grinding machine. The system is based on an optoelectronic measurement principle which makes highly accurate measurement at the nano-scale with a repeatability of ±0.1 μm possible.

The ultrasonic power supply converts 50 Hz electrical supply to high-frequency electrical impulses. These high-frequency electrical impulses are fed to a piezoelectric transducer and transformed into mechanical vibrations of ultrasonic frequency (20 kHz), due to the piezoelectric effect. The vibration amplitude is then amplified by the booster and the block sonotrode and transmitted to the workpiece fixed on the block sonotrode. The resultant vibration of the workpiece reaches 8 μm at a frequency of about 20 kHz. Vibration is applied to the workpiece in the feed direction of the grinding wheel. The amplitude of the ultrasonic vibration can be adjusted by changing the setting on the power supply.

The tests were carried out for both ultrasonic-assisted grinding (UAG) and conventional grinding (CG) with the same instrument. However, during the CG, the ultrasonic generator was switched off. It was important and necessary that investigation was carried out at the same tool condition. Therefore, the grinding wheel was sharpened using an aluminum oxide block before each series of the investigation. Therefore, it can be assumed that the wheel had identical initial topography. The sharpening process set the metal bond back, and thus, the worn and dull diamond grains fell out of the bond and new grains were liberated. In order to ensure protruding new abrasive layer, the outer wheel diameter was measured before and after the sharpening process, and the surface of the wheel was visually examined after the process.

The experimental equipment consists of the following:

Machine tool: Elb Micro-Cut AC8 CNC universal surface grinding machine
Surface roughness and profile tester: Hommel-Werke model T-8000
Dynamometer: Kistler piezoelectric dynamometer model 9255B
Nano-sensing device: Z-Nano HP by Novo Blum GmbH
Eddy current displacement measurement system: Micro-epsilon eddy NCDT 3,300, to measure the

Table 2 Resonance frequencies for the FEM modeling of the acoustic head

Modeling type	Polarized axis	Element type of piezoceramics	Element type of other components	Element size (mm)	Resonance frequency (kHz) from FEM modal	Measured resonance frequency (kHz)	% error	Time spent for modal analysis (min)
3D	*Z*	SOLID227	SOLID62	4	20.029	19.75	1.412	85
3D	*Z*	SOLID227	SOLID62	Smart size(2)	20.239	19.75	2.476	67

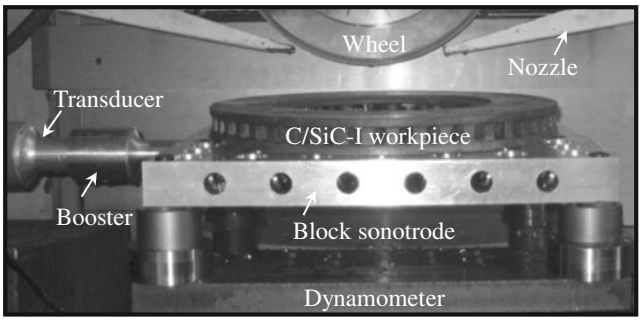

Fig. 6 The experimental setup

amplitude of vibration. Measuring ranges 0–0.5 mm, linearity 0.2%, resolution 0.005%, measuring rate 100 kHz

Ultrasonic vibration generator: AMMM-1,000 W generator-MP interconsulting, frequency ranges of 18.000 to 50 kHz

The settings of main machining parameters for the present study are summarized in Table 3.

Two different ceramic matrix composites, C/SiC-I and C/SiC-II, were used as the workpiece material in the grinding investigation. The C/SiC-I is a ceramic brake disk, made by one of famous manufacturers of carbon-based products, with three different layers: surface or the friction layer, glue layer, and C/C matrix or the basic material. It consists of a C/C core, SiC, and some free-Si. However, only the friction layer was grounded in this investigation. The C/SiC-II is also made by the same manufacturer but has only one layer, the friction layer. Compared with the C/SiC-I, the C/SiC-II consists of a much finer matrix, shortened and fewer carbon fibers per unit volume, significantly reduced free-Si in the matrix, and higher percentage of ceramic, SiC. The C/SiC-II has a higher hardness and lower fracture toughness than those of the C/SiC-I.

Investigations were carried out comparing conventional grinding with ultrasonic-assisted grinding. In order to achieve reliable data, each test was repeated three times. The influence of the cutting conditions, i.e., cutting speed and feed speed, and workpiece material and grinding process, i.e., CG and UAG, on the grinding forces, surface roughness, surface profile, and tool wear were studied. In the presented graphs, lines are formed by calculating the least-squares fit through the data points for a second-order polynomial equation.

3 Experimental results and discussion

Obtained results demonstrated an inverse relation between the vibration amplitude and the grinding forces and significantly reduced grinding forces at high amplitudes (Fig. 7), which correlates with previous findings [20–23]. Apparently, the reason for these improvements is the change of the nature of the cutting process, which is transformed into a process with a multiple-impact interaction between the abrasive grits and the workpiece. The larger the vibration amplitude, the higher the kinetic energy with which the grits strike the work surface. Regarding the kinematic of the process, increasing vibration amplitude increases the maximum cutting depth (or the maximum uncut chip thickness) and the infeed angle while decreasing the contact length (or chip length) and the contact time which result in an increased brittle material removal. Thus, it is clear that the effective tangential force acting on each single grain must fall. Due to the high-frequency interaction of active grains on the workpiece, the cutting process in ultrasonic-assisted grinding process becomes discontinuous and ultrasonic impact action occurs, thus causing the material to begin to rollover more easily as well as more micro-cracking propagation in the cutting zone which both make an effective interaction between grits and the workpiece surface [24, 25]. Therefore, the grinding forces and frictional effects are decreased, so that less plastic deformation occurs. In addition, as the sliding speed in the ultrasonic-assisted grinding process due to ultrasonic vibration is higher than the sliding speed in the conventional grinding process, the coefficient of friction reduces [21, 26].

In all the carried out experiments, normal grinding forces were higher than tangential grinding forces, and both normal and tangential forces were reduced by the ultrasonic-assisted grinding process. Figures 7 and 8 com-

Table 3 Major machining parameters

Grinding wheels	Metal bond diamond grinding wheel, D151, C118, Ø400×15 mm
Workpieces	C/SiC-I (1200 HV0.1) and C/SiC-II (1900 HV0.1)
Grinding conditions	Feed speed v_{ft}=0.5–3 m/min; cutting speed v_c=30–120 m/s; depth of cut a_e=0.050–0.6 mm
Grinding process	Surface grinding
Coolant	50 l/min, emulsion 5% (Syntilo XPS)
Sharpening conditions	Feed speed v_{ft}=2 m/min; cutting speed v_c=90 m/s; depth of cut a_e=4 mm, total depth of cut $a_{e\text{-total}}$=12 mm
Ultrasonic vibration	Parallel to the feed direction, frequency f=20 kHz, amplitude A=8 μm

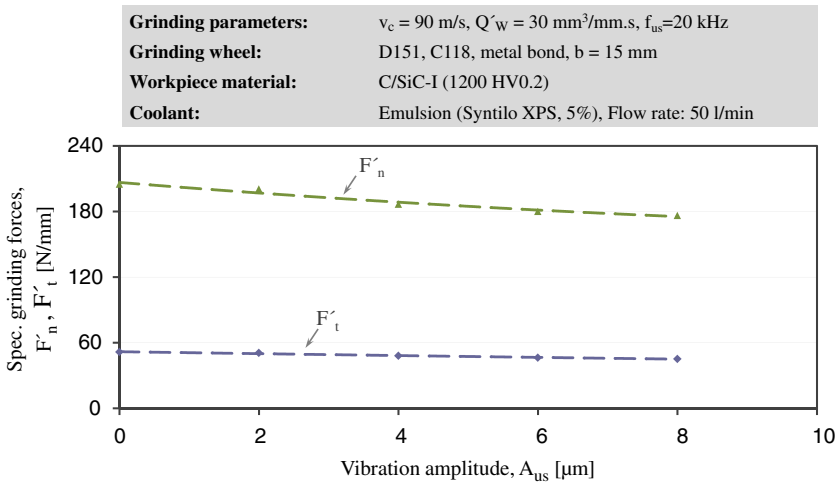

Fig. 7 Influence of the vibration amplitude on the specific grinding forces

pare the grinding forces and surface roughness produced by the UAG with the CG under different cutting speeds and feed speeds. It should be noted that the scatter in the measured surface roughness and grinding forces obtained through the UAG is less compared with the CG. It means that using UAG increases the repeatability of the grinding process. Superimposing ultrasonic vibration to the grinding process makes the process intermittent, enhancing coolant conduction and reducing the grinding temperature. It is well established, by the indentation fracture mechanics approach in ceramics, that the lateral extension of cracks occurs during indenter unloading [27]. These kinds of cracks are driven by a residual elastic/plastic mismatch stress field. Lateral cracks propagate laterally on a plane almost parallel to the specimen surface, and in a severe contact condition, they propagate toward the surface and induce material

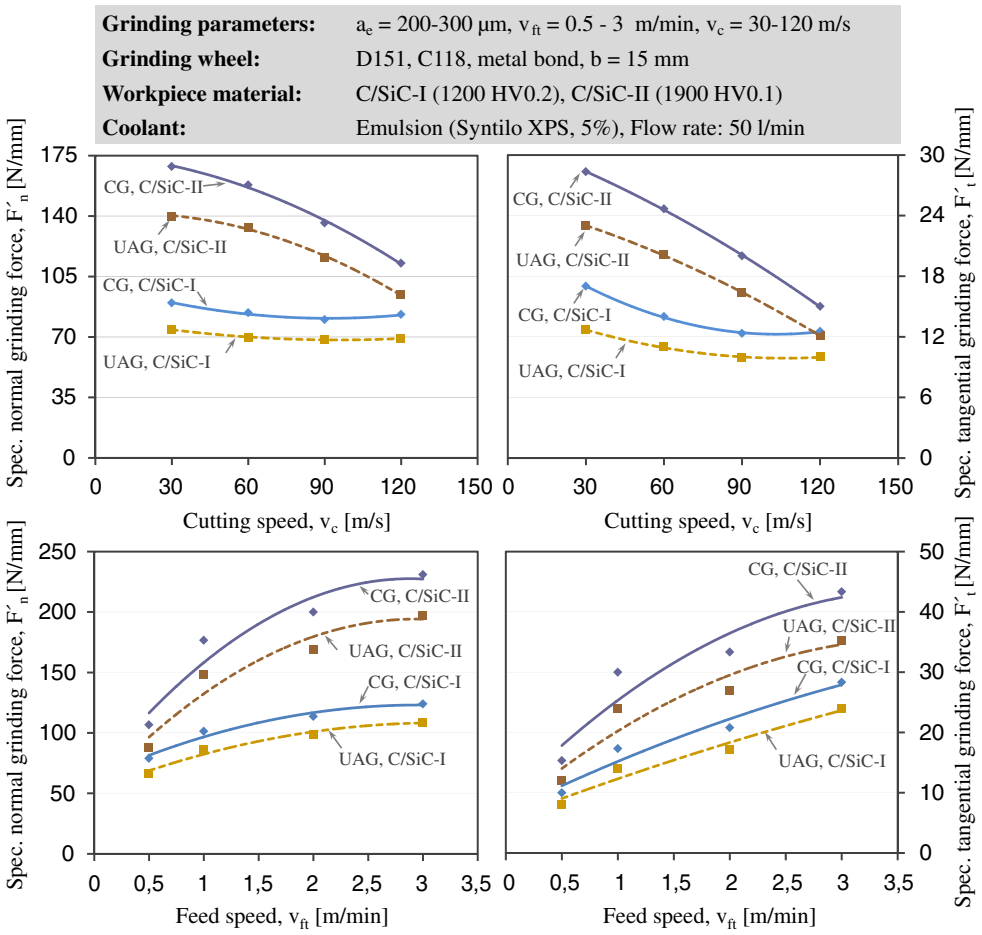

Fig. 8 Specific grinding forces as a function of the workpiece material, the grinding process, and **a** cutting speed, v_{ft}=1 m/min, a_e=200 µm; **b** feed speed, v_c=90 m/s, a_e=300 µm

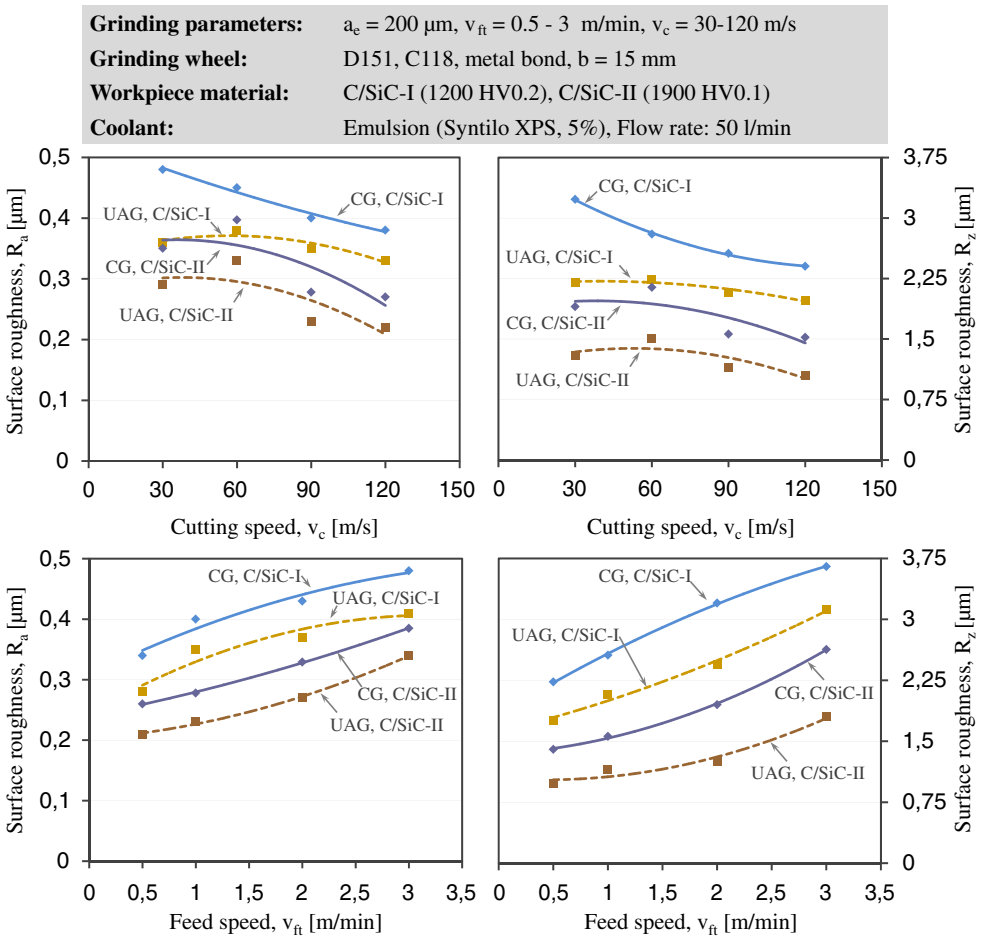

Fig. 9 Surface roughness as a function of the workpiece material, the grinding process, and **a** cutting speed, v_{ft}=1 m/min, a_e= 200 µm; **b** feed speed, v_c=90 m/s, a_e=200 µm

removal by fracture (chipping) [28]. Therefore, it is possible that the ultrasonic-assisted grinding process allows the lateral cracks to propagate and cause more micro-cracking propagation in the cutting zone and thus more brittle fracture and lower grinding forces.

As can be seen from Fig. 7, there is an inverse relation between the cutting speed and the grinding forces, i.e., increasing the cutting speed decreases the grinding forces. This trend is identical among both conventional (CG) and intermittent grinding process (IG). Increasing the cutting speed reduces the number of kinematic cutting edges and mean uncut chip thickness of each active grain. Hence, grinding forces acting on each active grain are decreased, resulting in a reduction of total grinding forces. Higher feed

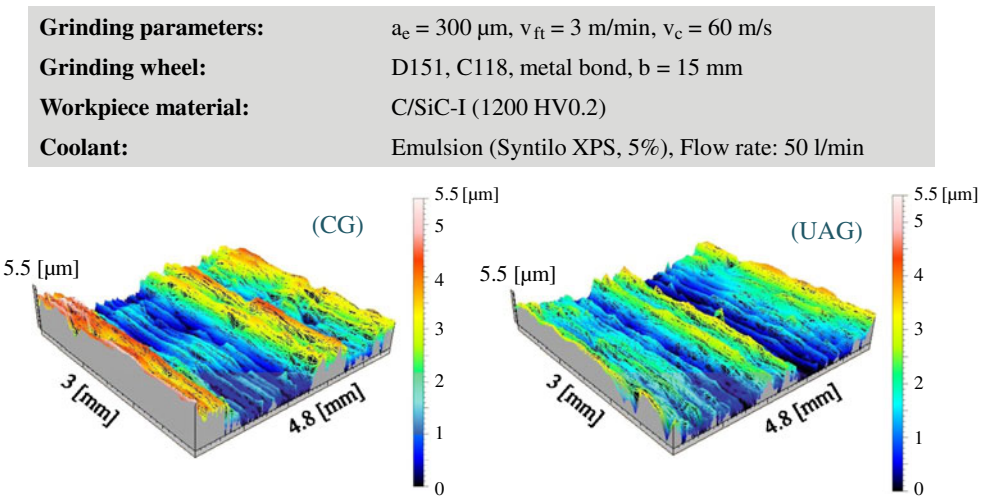

Fig. 10 3D surface topographies of the C/SiC-I ground surfaces. *Left* conventional grinding; *right* ultrasonic-assisted grinding (measured by the Hommel Tester T8000-tactile measurement)

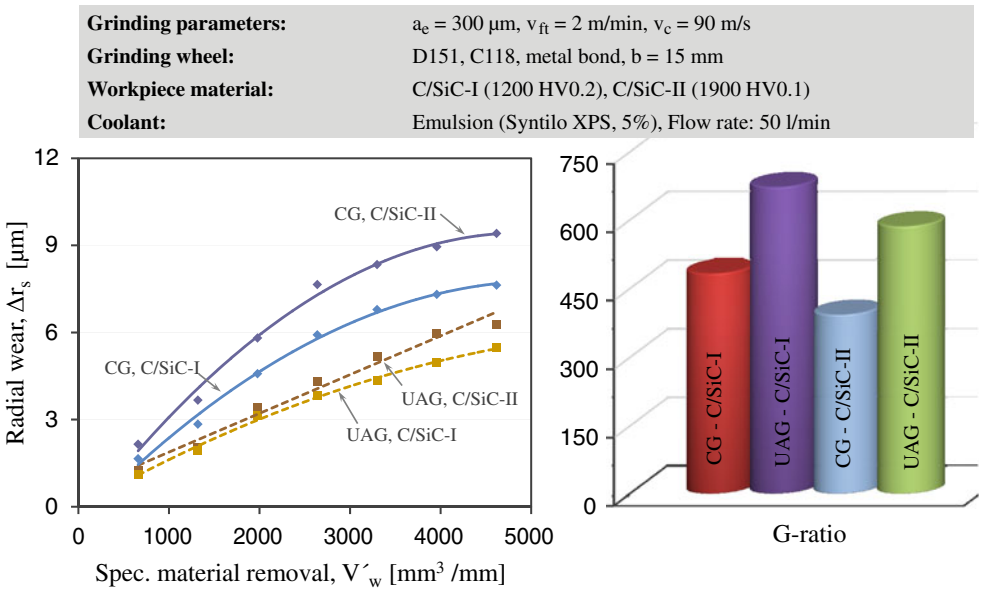

Fig. 11 Influence of the specific material removal and the grinding process on the radial wear and *G*-ratio

speeds cause an increased material removal rate and uncut chip thickness, resulting in higher normal and tangential forces. Additional to an increased uncut chip thickness, increasing feed speed increases the number of the kinematic cutting edges, inducing higher grinding forces [29].

Figure 7 shows that C/SiC-II material induces higher grinding forces than C/SiC-I. The very different grinding forces between C/SiC-II and C/SiC-I can be attributed to their dissimilar material properties. C/SiC-II hardness is around 1,900 HV0.1 and its flexural strength is about 140 MPa while C/SiC-I hardness is varied in the range of 1,080–1,400 HV0.2 and its flexural strength is around 80 MPa [9]. The wide range of C/SiC-I hardness is attributed to the presence of the carbon fiber, free silicon, and SiC together and a coarse matrix. Compared with C/SiC-I, C/SiC-II has a much higher hardness and flexural strength, causing diamond grain penetration into the workpiece to become harder and hence grinding forces become higher. In other words, C/SiC-II exhibits higher resistance to plowing and cutting. In addition, due to the higher flexural strength of C/SiC-II, superior stresses for inducing the cracks in the material are required [30].

Indicated by Fig. 8, the highest surface roughness values (both R_a and R_z) belong to the CG when grinding C/SiC-I material. Ultrasonic vibrations cause a reduction in friction because they apply an additional stress to assist in breaking the instantaneous welds, and they reduce the time that any two asperities on opposite surfaces can remain in momentary contact and hence keep them from forming a stronger weld. This suggests that in the ultrasonic-assisted grinding process, a fewer number of strong bonds between the grit and the material are formed, and the surface roughness is improved. Regarding Fig. 8, surface roughness increases with increasing feed speed and decreases at higher cutting

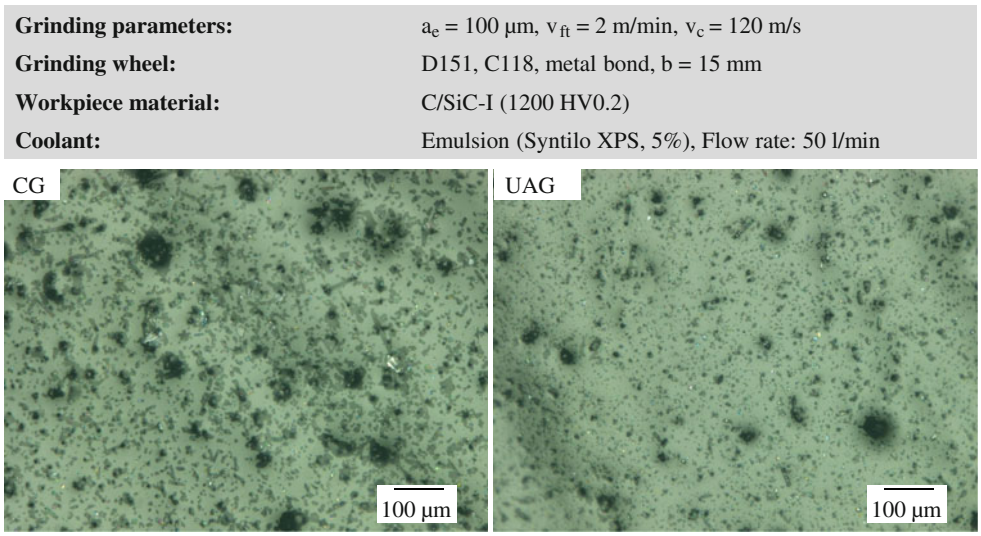

Fig. 12 A comparison between the grinding debris of the conventional grinding process (CG) and the ultrasonic-assisted grinding process with the normal wheel (UAG-N)

speeds. This general trend can be related to the influence of cutting speed and feed speed on the uncut chip thickness. Compared with C/SiC-II, C/SiC-I exhibits higher surface roughness. This is most probably due to the multitude micro cracks in the C/SiC-I matrix.

The 3D topography of surfaces produced by the utilized grinding are compared in Fig. 9. The surface produced by the ultrasonic-assisted grinding process is obviously finer and provides higher bearing ratios, i.e., ratio of bearing contact area to the total area, which is very important for the friction applications.

Radial wheel wear versus the specific material removal and the *G*-ratio for both the utilized grinding processes is presented in Fig. 10. Compared with UAG, CG has induced higher radial wear and lower *G*-ratio. Since the frictional effects between the abrasive cutting edges and the workpiece, grinding forces, and grinding temperatures are reduced by the ultrasonic-assisted grinding process, the abrasive grain experiences less wear and therefore the radial wear of the wheel will be reduced. Compared with C/SiC-I, the radial wear of the wheels is higher when grinding the C/SiC-II material. This behavior was expected since the C/SiC-II induces higher grinding forces.

The UAG makes the grinding process intermittent, helps cutting fluids to be brought into the contact zone, and enhances chips accommodation. During the period that the grinding wheel loses contact with the workpiece, the generated heat has time to spread and disperse. In other words, UAG allows heat to flow into the workpiece away from the cutting zone. Additionally, UAG reduces friction between the abrasive grains and the workpiece. Hence, the workpiece surface temperature is significantly reduced. Furthermore, the considerable force reduction by employing the UAG may also be interpreted as a reduction in the generated heat in the contact zone. Primary temperature measurements by the k-type thermocouples, at the KSF institute, demonstrated a significant reduction, of up to 25%, in the grinding temperatures in the case of UAG (compared with CG).

The mechanisms involved in material removal of a grinding process can be investigated by microscopic observation of the grinding debris. The microscopic examination of the collected grinding debris of both UAG and CG processes demonstrate that the former has generated debris a little shorter and finer than the debris produced by CG (Fig. 11). This is due to the effects of ultrasonic impact action, i.e., high-frequency interaction of active grains on the workpiece and the discontinuous cutting process in the ultrasonic-assisted grinding (Fig. 12).

Debris consists of particles with different size, type, and materials (Fig. 11). The carbon fiber and SiC particles can be distinguished from each other by their size, color, and shape. The carbon fiber particles are much larger than the SiC particles. They are black and appear to have fractured from the workpiece. The SiC particles are much finer than the carbon fiber particles and have grinding striations on one side. It is suggested that crushing or pulverization can be responsible for these fine particles [31–33].

4 Conclusion

An ultrasonic vibration system was invented which shows a multi-resonance behavior and makes it possible for the first time to vibrate heavy parts with different sizes, geometries, and weights. The influence of process variables, i.e., feed speed, cutting speed, vibration amplitude, and the influence of the workpiece material and the grinding process on the wear of the wheels, grinding forces, surface roughness, and debris, was investigated. The grinding forces were higher in the case of C/SiC-II compared with C/SiC-I. This phenomenon is attributed to the higher hardness of the former. Comparative experiments demonstrated a significant reduction in grinding forces (up to 20%) and surface roughness (up to 30%) for the workpieces machined with superimposed ultrasonic vibration. Compared with the conventional grinding process, the ground surface roughness and bearing ratio can be improved by the UAG.

References

1. Kazantsev VF (1979) Characteristic features of the plastic deformation of a material subjected to impact ultrasonic effects. AkustikaUl'trazvuk. Tekh., No. 15, pp 45–47
2. Markov AI (1980) Ultrasonic treatment of materials (in Russian). Mashinostroenie, Moscow
3. Nerubai MS (1987) Effect of ultrasonic vibrations on the mechanical properties of difficult-to-deform materials. Met Sci Heat Treat 29(4):254–258
4. Panin AV, Klimenov VA, Pochivalov YI, Son AA, Kazachenok MS (2004) The effect of ultrasonic treatment on mechanical behavior of titanium and steel specimens. Theor Appl Fract Mech 41:163–172
5. Severdenko P, Klubovichand VV, Stepanenko AV (1973) Pressure working of metals with ultrasound (in Russian). Nauka i Tekhnika, Minsk
6. Zhao B, Wu Y, Liu CS, Gaoand AH, Zhu XS (2006) The study on ductile removal mechanisms of ultrasonic vibration grinding nano-ZrO2 ceramics. Key Eng Mater 304–305:171–175
7. Zhao B, Wu Y, Jiao F, Gao GF, Zhu XS (2007) Experimental research on surface integrity of ceramic nanocomposites in two-dimensional ultrasonic vibration grinding. Key Eng Mater 329:445–450
8. Azarhoushang B, Tawakoli T (2009) Ultrasonicmachiningunit (in German), Deutsches Patent- und Markenamt, Aktenzeichen, 102009017248.3
9. Krenkel W (2008) Ceramic matrix composites. Wiley-VCH, Weinheim
10. Malkin S, Hwang T (1996) Grinding mechanisms for ceramics. Ann CIRP 45(2):569

11. Wagemann A (2001) Ceramic tools in metal forming (in German). Schmiedejournal
12. Li ZC, Jiao Y, Deines TW, Pei ZJ, Treadwell C (2005) Rotary ultrasonic machining of ceramic matrix composites: feasibility study and designed experiments. Int J Mach Tools Manuf 45:1402–1411
13. Tashiro T, Fujiwara J, Takenaka Y (2007) Grinding of C/C-SiC composite in dry method, in the book of towards synthesis of micro-/nano-systems, part 3. Springer, London, pp 351–352
14. Weinert K, Jansen T (2008) Machining aspects for the drilling of C/C-SiC materials. In: Krenkel W (ed) Ceramic matrix composites. Wiley-VCH, Weinheim, pp 287–301
15. Abdullah A, Pak A (2008) Correct prediction of the vibration behavior of the high power ultrasonic transducer by FEM simulation. Int J Adv Manuf Technol IJAMT 39(1–2):21–28
16. Azarhoushang B, Akbari J (2007) Ultrasonic-assisted drilling of Inconel 738-LC. Int J Mach Tools Manuf 47(7–8):1027–1033
17. Johnson DH, Pal D (2000) Simulation of an ultrasonic piezoelectric transducer. In: Proceedings of the 9th International ANSYS Conference, August 29
18. Prokic M (1997) A 1997 device for the generation of ultrasonic waves (in French). French patent application 2 743 929 (No d'enregistrement national: 9601029)
19. Prokic M (2001) Multifrequency ultrasonic structural actuator (MMM technology). European patent application, EP 1238715A1
20. Daus NA (2004) Ultrasonic assisted cross peripheral grinding (in German). Dissertation, Technische Universität Berlin
21. Tawakoliand T, Azarhoushang B (2008) Influence of ultrasonic vibrations on dry grinding of soft steel. Int J Mach Tools Manuf 48(14):1585–1591
22. Uhlmann E, Daus NA (2000) Ultrasonic assisted grinding—application advantages through an innovative grinding process (in German). BMBF-Abschlussbericht
23. Wu Y, Fan Y, Kato M, Kuriyagawa T, Syoji K, Tachibana T (2004) Development of an ultrasonic elliptic-vibration shoe centerless grinding technique. J Mater Process Technol 155–156:1780–1787
24. Cartsburg H (1993) Hard machining of ceramic composites (in German). Dissertation, Technische Universität Berlin
25. Qu W, Wang K, Miller MH, Huang Y, Chandra A (2000) Using vibration-assisted grinding to reduce subsurface damage. Precision Eng J 24:329–337
26. Frederick JR (1965) Ultrasonic engineering. Wiley, New York
27. Gordeev AV (1997) Wear resistance of segmental diamond wheels. Mach Tool (Eng translation Stanki Instrument) 48(2):21–22
28. Kim JD, Kang YH, Jin DX, Lee YS (1997) Development of discontinuous grinding wheel with multiporous grooves. Int J Mach Tools Manuf 37(11):1611–1624
29. Lawn BR, Evans AG, Marshall DB (1980) Elastic/plastic indentation damage in ceramics: the median/radial crack system. J Am Ceram Soc 63(9–10):574–581
30. Evans AG, Wilshaw TR (1976) Quasi-plastic solid particle damage in brittle materials. Acta Metall 24:939–956
31. Brown RH, Saito K, Shaw MC (1971) Local elastic deflections in grinding. Ann CIRP 19:105–113
32. Yamada T, Lee HS (2005) Study on elastic deformations of grinding wheels due to centrifugal forces by means of the grinding wheels model consisting of abrasive grains and bonds. J Jpn Soc Abrasive Technol JSAT 49(10):576–581
33. Puw HY, Hocheng H (1999) Milling of polymer composites. In: Jahanmir S, Ramulu M, Koshy P (eds) Machining of ceramics and composites. CRC, Boca Raton, pp 267–294